Siegert-state expansion for nonstationary systems. II. The whole-axis problem

Oleg I. Tolstikhin
Russian Research Center "Kurchatov Institute," Kurchatov Square 1, Moscow 123182, Russia
(Received 26 July 2006; published 18 October 2006)

An extension of the recently proposed approach [O. I. Tolstikhin, Phys. Rev. A **73**, 062705 (2006)] to the whole-axis problem is presented. Here, the motion in a one-dimensional time-dependent potential is considered. The solution to the time-dependent Schrödinger equation is expanded in terms of Siegert states. A set of coupled equations defining time evolution of the coefficients in the expansion is derived, in pseudodifferential and integral forms, and physical observables (probabilities of transitions to discrete states and the spectrum of ejected particles) are expressed in terms of these coefficients. The approach is implemented in terms of Siegert pseudostates and illustrated by calculations for a model system.

DOI: 10.1103/PhysRevA.74.042719 PACS number(s): 03.65.Nk, 31.15.−p, 31.70.Hq, 34.10.+x

I. INTRODUCTION

Expansion of the solution to the Schrödinger equation in terms of an appropriate basis, with subsequent reduction of the problem to a set of coupled equations in one variable, is a standard approach in scattering theory widely used both in time-dependent and stationary frameworks. Close-coupling methods not only provide a foundation for a great number of accurate computational studies of particular systems in atomic and molecular physics, but also underlie various approximate analytical adiabatic and semiclassical treatments. However, there remains one unresolved problem: usually close-coupling methods either completely neglect the continuum, or take it into account in an *ad hoc* way. Some may find this claim too strong, but probably nobody will argue that mathematical consistency and computational efficiency of close-coupling methods in treating transitions to discrete states is gone as soon as ionization is concerned.

A solution to this problem could be found in the use of Siegert states (SS) as a basis of the expansion. SS are eigenfunctions of the Hamiltonian having only one type of waves, incoming or outgoing, in the asymptotic region. These states were introduced in [1], which explains the name. The set of SS is purely discrete, which is an important advantage over the more familiar set of physical states that consists of discrete (bound states) and continuous (scattering states) parts. At the same time, the two sets can be uniquely expressed in terms of each other. Thus a close-coupling scheme based on the expansion in terms of SS should open a way to incorporate continuum on equal footing with discrete spectrum.

Even though the idea lies on the surface, only recently a first step in its realization has been made [2]. The main difficulty roots in rather unusual orthogonality and completeness properties of SS. It took time and effort to turn SS into an efficient tool for practical calculations. To this end, an algebraic approach and the concept of Siegert pseudostates (SPS) were introduced [3–5], without which further progress would not be possible. SPS have already found numerous applications in stationary scattering calculations [3–13]. Their applications in the time-dependent framework were pioneered in [14,15] and continued in [16] by studies of wave packet propagation in some model stationary systems. A generalization to the nonstationary case turned out to be nontrivial [2]. In this paper, the generic problem of *s*-wave scattering in a central time-dependent potential was considered. The solution to the time-dependent Schrödinger equation (TDSE) was expanded in terms of SS and a set of coupled equations defining time evolution of the coefficients in the expansion was derived. In contrast to other time-dependent close-coupling schemes, the resulting equations are pseudodifferential, which is a price for incorporating the continuum. Importantly, these equations treat the continuum with no approximation, unless the set is truncated for practical reasons. They were transformed to the form of coupled second kind Volterra integral equations which can be dealt with numerically almost as easily as ordinary differential equations. The approach was implemented in terms of SPS and illustrated by calculations.

In the radial problem considered in [2], the spatial variable is restricted to a half of the axis, with the zero boundary condition at the origin. In the present paper, the formulation of [2] will be extended to the whole-axis problem. The motivation of this work is twofold. First, although the extension is almost straightforward, the formulations are not identical. In particular, new aspects related to the possibility for the particle to be ejected in two opposite directions on the line appear, which requires a consideration. We shall omit details of the derivation where it parallels that in [2]. Second, the whole-axis problem essentially enriches possible physical applications. Thus, the interaction of a model one-dimensional atom with the electric field will be considered in the forthcoming paper [17]. The present work provides basic theory for such applications.

II. BASIC EQUATIONS

In this section, the TDSE will be presented in a matrix form suitable for expansion in terms of SS.

A. Formulation of the problem

We consider a particle moving in a one-dimensional time-dependent potential. The TDSE reads (a system of units in which all the quantities involved in the formulation are dimensionless and $\hbar=m=1$ is used throughout the paper)

$$i\frac{\partial\psi(x,t)}{\partial t} = H(t)\psi(x,t), \tag{1}$$

where

$$H(t) = H + U(x,t), \tag{2}$$

and

$$H = -\frac{1}{2}\frac{\partial^2}{\partial x^2} + V(x). \tag{3}$$

The potential here is divided into two parts: $V(x)$ is a stationary potential well and $U(x,t)$ represents the action of an external time-dependent force. It is assumed that both potentials have a finite range,

$$V(x)|_{x\leqslant x_-} = V(x)|_{x\geqslant x_+} = 0, \tag{4a}$$

$$U(x,t)|_{x\leqslant x_-} = U(x,t)|_{x\geqslant x_+} = 0. \tag{4b}$$

This is not a too restrictive assumption for $V(x)$, because any potential, probably except the Coulomb one, can be cutoff beyond a sufficiently large interval $x_-\leqslant x\leqslant x_+$ with no or little effect on the observables. The same is true for $U(x,t)$, if it represents, e.g., a time-dependent deformation of the potential well. More physically interesting problems, such as collisions (a particle in the field of two moving potential wells) and interaction with the electric field, also can be reduced to the form assumed in Eqs. (4), but this requires some additional transformation, see [17]. Here, we discuss only the basic problem, assuming that conditions (4) are satisfied. Another assumption concerns the behavior of $U(x,t)$ at large $|t|$,

$$U(x,t)|_{t\to\pm\infty} = 0. \tag{5}$$

Vanishing of $U(x,t)$ for $t\to-\infty$ means that the system was stationary in the infinite past. This allows us to formulate the initial condition for Eq. (1) in the form

$$\psi(x,t)|_{t\to-\infty} = e^{-iE_0t}\phi_0(x), \tag{6}$$

where $E_0<0$ and $\phi_0(x)$ correspond to a bound state in the potential $V(x)$,

$$\left[-\frac{1}{2}\frac{d^2}{dx^2} + V(x) - E_0\right]\phi_0(x) = 0, \tag{7a}$$

$$\phi_0(x)|_{x\to\pm\infty} = 0. \tag{7b}$$

Taking into account Eq. (4a) we have

$$\phi_0(x)|_{x\leqslant x_-} = \phi_0(x_-)e^{-ik_0(x-x_-)}, \tag{8a}$$

$$\phi_0(x)|_{x\geqslant x_+} = \phi_0(x_+)e^{+ik_0(x-x_+)}, \tag{8b}$$

where $k_0=i\sqrt{-2E_0}$. In order that one could define observables, potential $U(x,t)$ must become independent of time for $t\to\infty$; the present more stringent assumption that $U(x,t)$ vanishes for $t\to\infty$ is not essential and can be relaxed. The problem consists in finding the observables, i.e., the probabilities of transitions to discrete states and the spectrum of ejected particles.

B. Matrix form of the time-dependent Schrödinger equation

Let us introduce some notation. The function and derivative value operators at $x=x_0$ are defined by

$$\mathcal{F}(x_0) = \delta(x-x_0), \quad \mathcal{D}(x_0) = \delta(x-x_0)\frac{d}{dx}. \tag{9}$$

Following Bloch [18], we introduce hermitized Hamiltonians,

$$\tilde{H} = H + \frac{1}{2}[\mathcal{D}(x_+) - \mathcal{D}(x_-)], \tag{10}$$

$$\tilde{H}(t) = H(t) + \frac{1}{2}[\mathcal{D}(x_+) - \mathcal{D}(x_-)]. \tag{11}$$

Following [2], we introduce a pseudodifferential operator $\hat{\lambda}_t$ whose action on a function

$$f(t) = \int_{-\infty}^{\infty} f(E)e^{-iEt}\frac{dE}{2\pi} \tag{12}$$

is defined by

$$\hat{\lambda}_t f(t) = \int_{-\infty}^{\infty} ikf(E)e^{-iEt}\frac{dE}{2\pi}. \tag{13}$$

In this paper, E and k always denote energy and momentum related to each other by

$$E = \frac{1}{2}k^2, \quad k = \sqrt{2E}, \tag{14}$$

where the branch of the square root function for which $\mathrm{Im}\,k>0$ on the physical sheet of E is meant. As usual in the scattering theory [19], it is understood that the integration path in Eqs. (12) and (13) lies on the physical sheet infinitesimally above the real axis. From Eqs. (14) one finds that $\hat{\lambda}_t$ is related to the time derivative by

$$i\frac{\partial}{\partial t} = -\frac{\hat{\lambda}_t^2}{2}, \quad -i\hat{\lambda}_t = \sqrt{2i\frac{\partial}{\partial t}}. \tag{15}$$

For a more detailed discussion of this operator and some of its properties see [2].

It can be shown [2] that the solution to Eqs. (1) and (6) satisfies the outgoing wave boundary conditions,

$$\frac{\partial\psi(x,t)}{\partial x} = -\hat{\lambda}_t\psi(x,t), \quad x\leqslant x_-, \tag{16a}$$

$$\frac{\partial\psi(x,t)}{\partial x} = +\hat{\lambda}_t\psi(x,t), \quad x\geqslant x_+, \tag{16b}$$

which means that there are only waves going to the left and right in the left, $x<x_-$, and right, $x>x_+$, outer regions, respectively. As a consequence of Eqs. (16) we have

$$\mathcal{D}(x_\pm)\psi(x,t) = \pm\mathcal{F}(x_\pm)\hat{\lambda}_t\psi(x,t). \tag{17}$$

Using these relations, Eq. (1) can be presented in a matrix form

$$\left[\hat{\lambda}_t - \begin{pmatrix} 0 & 1 \\ -2\tilde{H}(t) & \mathcal{F} \end{pmatrix}\right]\begin{pmatrix} \psi(x,t) \\ \tilde{\psi}(x,t) \end{pmatrix} = 0, \tag{18}$$

where $\tilde{\psi}(x,t)=\hat{\lambda}_t\psi(x,t)$ and

$$\mathcal{F} = \mathcal{F}(x_-) + \mathcal{F}(x_+). \tag{19}$$

Equation (18) coincides with Eq. (34) from [2], but the definition of $\mathcal{F}$ is different.

III. SIEGERT STATES: STATIONARY SCATTERING THEORY

The solution to Eq. (18) will be sought as an expansion in terms of SS for the stationary Hamiltonian (3). So far, the theory of SS has been developed using the algebraic approach, i.e., in terms of SPS, only for one- [4] and two-channel [5] radial problems. An extension to the whole-axis problem in the case when the asymptotic values of potential $V(x)$ at $x\to\pm\infty$ coincide (degenerate thresholds) can be straightforwardly obtained from the one-channel theory [4], see the appendix in [7]. We mention that the general case of nondegenerate thresholds is also covered by a mapping to the two-channel problem [5], see [12]. In this section, we summarize basic results of the theory of SS needed for the following discussion.

The SS are defined by

$$(H-E)\phi(x) = 0, \tag{20a}$$

$$\left(\frac{d}{dx} \mp ik\right)\phi(x)\bigg|_{x=x_\pm} = 0. \tag{20b}$$

This is an eigenvalue problem; the SS momentum and energy eigenvalues and eigenfunctions will be denoted by k_n, $E_n=k_n^2/2$, and $\phi_n(x)$, respectively. Equations (20) can be presented in a matrix form similar to Eq. (18),

$$\left[\begin{pmatrix} 0 & 1 \\ -2\tilde{H} & \mathcal{F} \end{pmatrix} - ik_n\right]\begin{pmatrix} \phi_n(x) \\ \tilde{\phi}_n(x) \end{pmatrix} = 0, \tag{21}$$

where $\tilde{\phi}_n(x)=ik_n\phi_n(x)$. Acting as in [2], one can show that the solutions to Eq. (21) are orthogonal with respect to the inner product

$$\int_{x_-}^{x_+} \phi_n(x)\phi_m(x)dx + i\frac{\phi_n(x_-)\phi_m(x_-) + \phi_n(x_+)\phi_m(x_+)}{k_n + k_m} = \delta_{nm}, \tag{22}$$

and satisfy the following completeness relations:

$$\sum_n \frac{1}{ik_n}\phi_n(x)\phi_n(x') = 0, \tag{23a}$$

$$\sum_n \phi_n(x)\phi_n(x') = 2\delta(x-x'), \tag{23b}$$

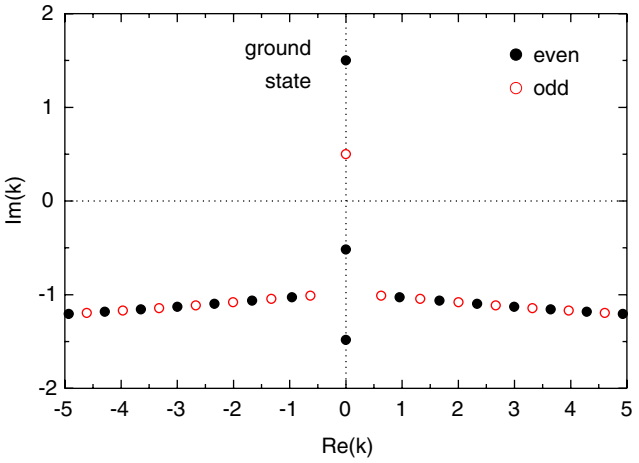

FIG. 1. (Color online) SS momentum eigenvalues k_n for the Eckart potential (49) with cutoff distances $-x_-=x_+=5$.

$$\sum_n ik_n\phi_n(x)\phi_n(x') = 2[\delta(x-x_-)\delta(x'-x_-) + \delta(x-x_+)\delta(x'-x_+)]. \tag{23c}$$

A difference between Eqs. (22) and (23) and their counterparts in [2] is explained by a difference in the definition of $\mathcal{F}$, see Eq. (19). For symmetric potentials, $V(x)=V(-x)$, the eigenfunctions $\phi_n(x)$ are either even or odd functions of x. A typical distribution of SS momentum eigenvalues k_n in the complex plane is shown in Fig. 1.

The central object in the stationary scattering theory, the outgoing wave Green's function, is defined by

$$(E-H)G(x,x';k) = \delta(x-x'), \tag{24a}$$

$$\left(\frac{d}{dx} + ik\right)G(x,x';k)\bigg|_{x=x_-} = 0, \quad x' > x_-, \tag{24b}$$

$$\left(\frac{d}{dx} - ik\right)G(x,x';k)\bigg|_{x=x_+} = 0, \quad x' < x_+. \tag{24c}$$

Using Eqs. (20) and (23), one can obtain its expansion in terms of SS,

$$G(x,x';k) = \sum_n \frac{\phi_n(x)\phi_n(x')}{k_n(k-k_n)}, \quad x_- \leqslant x,x' \leqslant x_+, \tag{25}$$

in full analogy with [2].

The set of SS is in one-to-one correspondence with the set of physical states for the same Hamiltonian (3). The bound states of H are given by the SS for which $\mathrm{Re}\,k_n=0$ and $\mathrm{Im}\,k_n>0$, see Fig. 1. The set of subscripts n corresponding to bound SS will be denoted by $\{b\}$. We shall assume that the bound state in the initial condition (6) is given by the SS with $n=0\in\{b\}$. All the other SS serve to represent the continuum. Let $\varphi_\pm^{\mathrm{in}}(x,k)$, $0\leqslant k<\infty$, be the solutions to Eq. (20a) satisfying boundary conditions

$$\varphi_-^{\mathrm{in}}(x,k) = \begin{cases} e^{ikx} - r_-(k)e^{-ikx}, & x \leqslant x_-, \\ t(k)e^{ikx}, & x \geqslant x_+, \end{cases} \tag{26a}$$

$$\varphi_+^{\text{in}}(x,k) = \begin{cases} t(k)e^{-ikx}, & x \leqslant x_-, \\ e^{-ikx} - r_+(k)e^{ikx}, & x \geqslant x_+, \end{cases} \tag{26b}$$

where $r_\pm(k)$ and $t(k)$ are the reflection and transmission amplitudes. These coefficients are related by $r_-(k)t^*(k) + r_+^*(k)t(k) = 0$; for symmetric potentials, $r_-(k) = r_+(k)$. A new feature compared to the radial case [2] is that scattering states in the whole-axis problem are doubly degenerate. Therefore, one can introduce different sets of scattering states. Of particular importance in the time-dependent framework are *in* and *out* states [19]. The states defined by Eqs. (26) are *in* states; the wave packets formed by a superposition of $\varphi_-^{\text{in}}(x,k)$ and $\varphi_+^{\text{in}}(x,k)$ from a narrow interval of $k > 0$ in the remote past approach the interaction region $x_- \leqslant x \leqslant x_+$ from the left and right, respectively. To define the observables, we shall need *out* states $\varphi_\pm^{\text{out}}(x,k)$; the wave packets formed from $\varphi_-^{\text{out}}(x,k)$ and $\varphi_+^{\text{out}}(x,k)$ in the remote future recede from the interaction region to the left and right, respectively. The two sets of scattering states are related by a unitary transformation,

$$\begin{pmatrix} \varphi_-^{\text{out}}(x,k) \\ \varphi_+^{\text{out}}(x,k) \end{pmatrix} = \begin{pmatrix} -r_-^*(k) & t^*(k) \\ t^*(k) & -r_+^*(k) \end{pmatrix} \begin{pmatrix} \varphi_-^{\text{in}}(x,k) \\ \varphi_+^{\text{in}}(x,k) \end{pmatrix}. \tag{27}$$

It can be easily seen that

$$\varphi_\pm^{\text{out}}(x,k) = \varphi_\pm^{\text{in}*}(x,k). \tag{28}$$

Together with the bound states, each type of scattering states form a complete set,

$$\sum_{n\in\{b\}} \phi_n(x)\phi_n(x') + \int_0^\infty [\varphi_-^*(x,k)\varphi_-(x',k) + \varphi_+^*(x,k)\varphi_+(x',k)]\frac{dk}{2\pi} = \delta(x-x'), \tag{29}$$

where we have omitted superscripts "in" and "out."

Scattering states also can be expanded in terms of SS. Consider, e.g., *in* states. We have

$$G(x,x';k) = \frac{-i}{kt(k)}\varphi_-^{\text{in}}(x_>,k)\varphi_+^{\text{in}}(x_<,k), \tag{30}$$

where $x_>$ ($x_<$) is the larger (the smaller) of x and x'. Hence

$$\varphi_-^{\text{in}}(x,k) = ike^{+ikx_-}G(x,x_-;k), \quad x \geqslant x_-, \tag{31a}$$

$$\varphi_+^{\text{in}}(x,k) = ike^{-ikx_+}G(x,x_+;k), \quad x \leqslant x_+. \tag{31b}$$

Substituting here expansion (25) one obtains

$$\varphi_\pm^{\text{in}}(x,k) = ike^{\mp ikx_\pm}\sum_n \frac{\phi_n(x)\phi_n(x_\pm)}{k_n(k-k_n)}, \quad x_- \leqslant x \leqslant x_+. \tag{32}$$

Comparing this with Eqs. (26) one finds

$$r_\pm(k) = e^{\mp 2ikx_\pm}\left[1 - ik\sum_n \frac{[\phi_n(x_\pm)]^2}{k_n(k-k_n)}\right], \tag{33a}$$

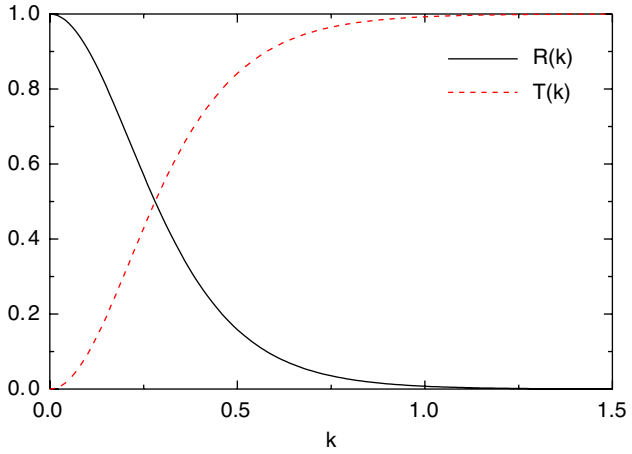

FIG. 2. (Color online) Reflection $R(k) = |r_-(k)|^2 = |r_+(k)|^2$ and transmission $T(k) = |t(k)|^2$ coefficients for the Eckart potential (49) obtained from Eqs. (33).

$$t(k) = ike^{ik(x_- - x_+)}\sum_n \frac{\phi_n(x_-)\phi_n(x_+)}{k_n(k-k_n)}. \tag{33b}$$

These formulas complete the SS formulation of the stationary scattering theory for the present case. The reflection and transmission coefficients obtained from Eqs. (33) for the same potential as in Fig. 1 are shown in Fig. 2.

IV. SIEGERT-STATE EXPANSION

The solution to Eqs. (1) and (6) can be expanded in terms of the SS discussed above. In this section, we derive equations defining time evolution of the coefficients in the expansion and express observables in terms of these coefficients.

A. Inner region: Coupled equations for the coefficients

The solution to Eq. (18) in the inner region can be sought in the form

$$\begin{pmatrix} \psi(x,t) \\ \tilde{\psi}(x,t) \end{pmatrix} = \sum_n a_n(t)\begin{pmatrix} \phi_n(x) \\ \tilde{\phi}_n(x) \end{pmatrix}, \quad x_- \leqslant x \leqslant x_+. \tag{34}$$

Acting as in [2] and using the above results, one obtains a set of coupled pseudodifferential equations for the coefficients,

$$ik_n(\hat{\lambda}_t - ik_n)a_n(t) + \sum_m U_{nm}(t)a_m(t) = 0, \tag{35a}$$

$$a_n(t)|_{t\to-\infty} = \delta_{n0}e^{-iE_0t}, \tag{35b}$$

where

$$U_{nm}(t) = \int_{x_-}^{x_+} \phi_n(x)U(x,t)\phi_m(x)dx. \tag{36}$$

Using the retarded Green's function $g(t;k)$ for the operator $\hat{\lambda}_t - ik$, see [2], one can rewrite Eqs. (35) in an integral form,

$$a_n(t) = \delta_{n0}e^{-iE_0t} + \frac{i}{k_n}\sum_m \int_{-\infty}^{t} g(t-t';k_n)U_{nm}(t')a_m(t')dt'. \tag{37}$$

These are inhomogeneous Volterra equations of the second kind; they incorporate the initial conditions (35b). Solving Eqs. (35) or (37), one finds $\psi(x,t)$ in the inner region.

B. Wave function in the outer region

In the outer regions, any solution to Eq. (1) satisfying the outgoing wave boundary conditions (16) is given by

$$\psi(x,t) = \int_{-\infty}^{\infty} c_-(E)e^{-ikx-iEt}\frac{dE}{2\pi}, \quad x \leqslant x_-, \tag{38a}$$

$$\psi(x,t) = \int_{-\infty}^{\infty} c_+(E)e^{+ikx-iEt}\frac{dE}{2\pi}, \quad x \geqslant x_+. \tag{38b}$$

Requiring continuity of $\psi(x,t)$ at $x=x_\pm$, one obtains

$$c_\pm(E) = e^{\mp ikx_\pm}\int_{-\infty}^{\infty} \psi(x_\pm,t)e^{iEt}dt. \tag{39}$$

Thus $\psi(x,t)$ in the outer regions is given in terms of $\psi(x_\pm,t)$ which, in turn, are given in terms of $a_n(t)$ by Eq. (34).

C. Observables

Coefficients $a_n(t)$ in Eq. (34) do not have that simple a meaning as the coefficients in expansions in terms of physical states. In particular, $|a_n(t)|^2$ does not give the probability to find the system in the nth SS; one should remember that all but the bound SS are not even normalizable in the ordinary sense of the word. To find observables, one has to re-expand the solution to Eqs. (1) and (6) in terms of the *out* set of physical states,

$$\psi(x,t) = \sum_{n\in\{b\}} C_n(t)\phi_n(x) + \int_0^{\infty} [C_-(k,t)\varphi_-^{\text{out}}(x,k) + C_+(k,t)\varphi_+^{\text{out}}(x,k)]\frac{dk}{2\pi}. \tag{40}$$

The coefficients here are given by

$$C_n(t) = \int_{-\infty}^{\infty} \phi_n(x)\psi(x,t)dx = \sum_m a_m(t) \times\left[\delta_{nm} - i\frac{\phi_n(x_-)\phi_m(x_-)+\phi_n(x_+)\phi_m(x_+)}{k_n+k_m}\right] - \int_{-\infty}^{\infty} g(t-t';-k_n)[\phi_n(x_-)\psi(x_-,t') + \phi_n(x_+)\psi(x_+,t')]dt', \tag{41a}$$

$$C_\pm(k,t) = \int_{-\infty}^{\infty} \varphi_\pm^{\text{out}*}(x,k)\psi(x,t)dx = -\int_{-\infty}^{\infty} t(k)e^{\mp ikx_\mp}g(t-t';-k)\psi(x_\mp,t')dt' + ike^{\mp ikx_\pm}\sum_{n,m}\frac{\phi_n(x_\pm)a_m(t)}{k_n(k-k_n)} \times\left[\delta_{nm} - i\frac{\phi_n(x_-)\phi_m(x_-)+\phi_n(x_+)\phi_m(x_+)}{k_n+k_m}\right] - \int_{-\infty}^{\infty} [e^{\mp ikx_\pm}g(t-t';k) - r_\pm(k)e^{\pm ikx_\pm} \times g(t-t';-k)]\psi(x_\pm,t')dt'. \tag{41b}$$

Again acting as in [2], one finds

$$C_n(t)|_{t\to\infty} = C_n e^{-iE_nt}, \tag{42a}$$

$$C_\pm(k,t)|_{t\to\infty} = C_\pm(k)e^{-iEt}, \tag{42b}$$

where

$$C_n = \delta_{n0} - i\sum_m \int_{-\infty}^{\infty} e^{iE_nt}U_{nm}(t)a_m(t)dt, \tag{43a}$$

$$C_\pm(k) = ke^{\mp ikx_\pm}\int_{-\infty}^{\infty} \psi(x_\pm,t)e^{iEt}dt. \tag{43b}$$

Note that $C_\pm(k)=kc_\pm(E)$, as one could expect from Eqs. (38) and (39). Summarizing, the observables, i.e., probabilities P_n to find the system in bound states $n\in\{b\}$ and momentum distributions of particles ejected to the left, $P_-(k)$, and right, $P_+(k)$, are given by

$$P_n \equiv |C_n|^2 = |\delta_{n0} - iA_n(E_n)|^2, \tag{44a}$$

$$P_\pm(k) \equiv |C_\pm(k)|^2 = k^2\left|\sum_n \frac{A_n(E)}{k_n(k-k_n)}\phi_n(x_\pm)\right|^2, \tag{44b}$$

where

$$A_n(E) = \sum_m \int_{-\infty}^{\infty} e^{iEt}U_{nm}(t)a_m(t)dt. \tag{45}$$

Apart from two possible directions of ionization represented by subscripts $\pm$, these formulas look similar to the corresponding results in [2]. The normalization of the wave function $\psi(x,t)$ and unitarity lead to

$$\int_{-\infty}^{\infty} |\psi(x,t)|^2dx = \sum_{n\in\{b\}} P_n + \int_0^{\infty} [P_-(k)+P_+(k)]\frac{dk}{2\pi} = 1. \tag{46}$$

The distribution of ejected particles in energy is given by

$$P(E) = \frac{P_-(k)+P_+(k)}{2\pi k}, \tag{47}$$

and the total probability of ionization is

$$P_{\text{ion}} = \int_0^\infty P(E)dE. \tag{48}$$

V. ILLUSTRATIVE EXAMPLES

In this section, we illustrate the approach by numerical calculations. While the purpose of the numerical illustrations in [2] was only to demonstrate the principle feasibility of the approach, here we discuss a more physically motivated model.

A. The model

We consider a particle in the Eckart potential well

$$V(x) = -\frac{15/8}{\cosh^2 x}. \tag{49}$$

Strictly speaking, this potential does not satisfy condition (4a). However, from the physical viewpoint, it is clear that cutting off its exponentially decaying tails at a sufficiently large distance $|x|=X$ should not produce any effect on the observables. In the calculations we shall use the cutoff potential, with the understanding that convergence of the results with respect to the cutoff radius X must be achieved. In stationary scattering calculations, this convergence is rather fast and similar to that in the radial problem, see the examples discussed in [4]. Potential (49) supports two bound states with energies $E_0=-9/8$ and $E_1=-1/8$, see Fig. 1. These SS eigenvalues rapidly converge as X grows; our calculations with $X=5$ reproduce eleven digits in E_0 and seven digits in E_1. Even though all the other SS eigenvalues essentially depend on X, the reflection and transmission amplitudes calculated from Eqs. (33) rapidly converge; the results obtained with $X=5$, see Fig. 2, are correct to about six significant digits. This level of accuracy is more than sufficient for the present illustrative purposes, so in the calculations we put $-x_-=x_+=X=5$.

One of the most interesting applications of the present approach lies in the field of laser-atom interaction. This corresponds to the time-dependent potential of the form

$$U(x,t) = -xF_0 f(t), \tag{50}$$

where F_0 is the amplitude of the electric field pulse and function $f(t)$ describes its shape in time. Potential (50) also does not satisfy condition (4b). To bring it to the form assumed in the formulation given above, we introduce the cutoff potential

$$U_c(x,t) = U(x,t)\theta(X - |x|). \tag{51}$$

However, in contrast to the case with $V(x)$, cutting off the electric field beyond $|x|=X$ may essentially modify the dynamics. This difficulty will be resolved in [17], where the full potential (50) will be exactly incorporated in the formulation. In the present calculations we use the cutoff potential (51). The difference between $U(x,t)$ and $U_c(x,t)$ should not reveal itself in the situations when the observables are determined only by matrix elements involving the initial bound state, because the contribution to such matrix elements from the outer region $|x|>X$ is exponentially small. There are three such situations: perturbation theory, sudden approximation, and rotating wave approximation in a resonant field. We shall consider each of them, thus demonstrating the approach in the very different regimes, but without departing too far from the physically meaningful model (50). So, the discussion below should be viewed as a preliminary step toward the analysis of [17]. Alternatively, one can notice that Eq. (51) represents the electric field in a condensator, which is another model that may be of interest by itself. In any case, we recall that our goal here is only to illustrate the approach.

In all the calculations below, we take the ground state in the potential (49) as the state 0 in the initial condition (6); the only excited bound state will be denoted by 1. The approach was implemented in terms of SPS. The numerical results were obtained by solving integral equations (37) using the algorithm described in [2]. We focus on ionization because this is where advantages of the present approach are expected to be most pronounced.

B. Perturbative regime: Above-threshold ionization

Consider ionization by a small amplitude pulse with the shape

$$f(t) = \begin{cases} \sin^2(\pi t/T)\cos\omega t, & 0 \leqslant t \leqslant T, \\ 0, & \text{otherwise}. \end{cases} \tag{52}$$

The first-order perturbation theory result for $P_\pm(k)$ reads [20]

$$P_\pm^{PT}(k) = |F_0 d_\pm^c(k) f(E - E_0)|^2, \tag{53}$$

where $d_\pm^c(k)$ is the matrix element for the potential (51),

$$d_\pm^c(k) = \int_{-X}^{X} \varphi_\pm^{\text{out}^*}(x,k) x \phi_0(x) dx, \tag{54}$$

and $f(E)$ is the Fourier transform of $f(t)$. For $\omega=n\omega_0$, $n=0,1,\ldots$, $\omega_0=2\pi/T$, we have

$$f(E) = \frac{-e^{iET/2}\sin(ET/2)E\omega_0^2(E^2+3\omega^2-\omega_0^2)}{[(E-\omega)^2-\omega_0^2](E^2-\omega^2)[(E+\omega)^2-\omega_0^2]}. \tag{55}$$

For large n, this function has a sharp peak at $E=\omega$ with the height $f(\omega)=T/4$ and width $\sim\omega_0=\omega/n$, so the pulse becomes monochromatic as $n\to\infty$. The calculations were done with $F_0=0.1$, $T=200$, and $n=100$, hence $\omega=\pi$. The numerical and perturbation theory results are compared in Figs. 3 and 4.

Because of the symmetry of potential (49), from Eq. (53) we have $P_-^{PT}(k)=P_+^{PT}(k)$. This prediction of perturbation theory is confirmed by the calculations: the results for $P_-(k)$ and $P_+(k)$ virtually coincide. In this case, instead of $P_\pm(k)$ it is more convenient to consider the distribution of ejected particles in energy (47). The probability of excitation $P_1=1.95\times10^{-12}$ and the total probability of ionization $P_{\text{ion}}=1.63\times10^{-3}$ obtained from the calculations are sufficiently small for perturbation theory to be quantitatively correct. Indeed, one can see a perfect agreement between the numerical and perturbation theory results in Fig. 3. The

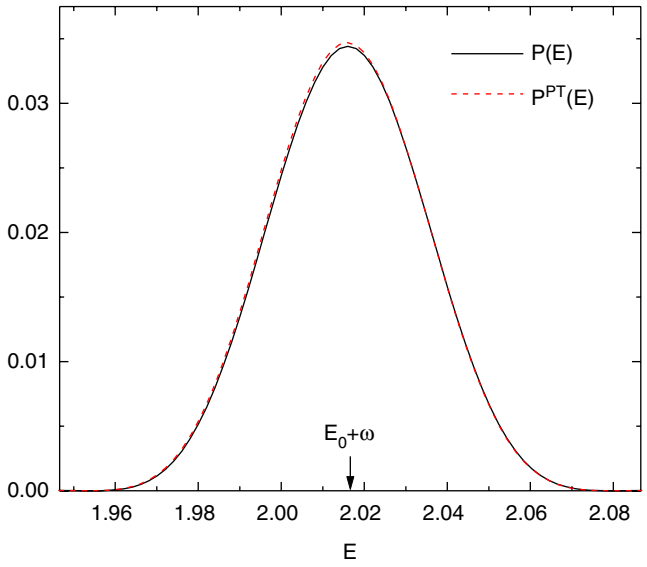

FIG. 3. (Color online) Comparison of the calculated $P(E)$ and perturbation theory $P^{PT}(E)$ results for the spectrum of ejected particles near the one-photon absorption energy $E=E_0+\omega$.

shape of the spectrum is determined by function (55), the matrix element $d_{\pm}^{c}(k)$ being almost constant within the width of the peak in Fig. 3. The maximum of $P^{PT}(E)$ lies at $E=2.015\,84$, which is close to the one-photon absorption energy $E_0+\omega=2.016\,59$; the difference being due to a finite spectral width of the pulse. The maximum of the calculated spectrum $P(E)$ lies at $E=2.016\,04$, i.e., is shifted with respect to that of $P^{PT}(E)$ by 2.0×10^{-4} toward higher energies. The latter difference is attributed to the dynamical Stark shift for the ground state, which can be roughly estimated as $F_0^2/4\omega^2\approx2.5\times10^{-4}$ [21]. Thus even such a tiny effect is reproduced by the calculations. The one-photon peak in Fig. 3 is the only feature seen in the spectrum in the linear scale, the contribution to P_{ion} from other energies is negligible.

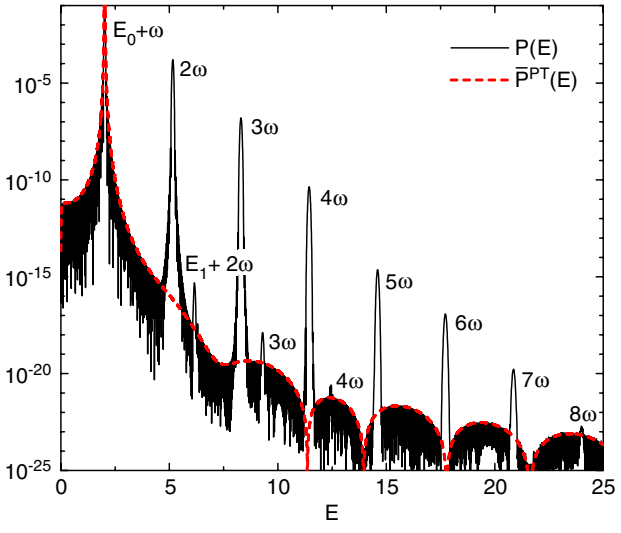

FIG. 4. (Color online) Same as in Fig. 2, but in a wider energy range. Here $\bar{P}^{PT}(E)$ is the envelope of the perturbation theory results obtained by dropping the rapidly oscillating factor $\sin(ET/2)$ in Eq. (55). One can clearly see a number of ATI peaks produced by multiphoton absorption from the ground and excited states.

Let us consider the same spectrum in a wider energy range and in the logarithmic scale, see Fig. 4. Rapid oscillations of the calculated results are explained by the factor $\sin(ET/2)$ in Eq. (55). To compare with perturbation theory, we drop this factor, i.e., the dashed curve in Fig. 4 gives the envelope of the spectrum obtained from Eq. (53). The first feature to be pointed out in Fig. 4 is a series of profound above-threshold ionization (ATI) peaks [22] corresponding to absorption of two or more photons from the ground state (the one-photon peak in Fig. 3 is the first member of the series). These peaks are beyond the first order of perturbation theory, of course, but are reproduced by the calculations. The heights of n-photon peaks decay $\propto F_0^{2n}$, as they should in the perturbative regime. The second feature is clearly visible peaks corresponding to absorption of two, three, and four photons from the excited state. These peaks are lower by about a factor of P_1 than corresponding peaks for ionization from the ground state, which indicates that they are produced by absorbing one additional photon with energy E_1-E_0 (such photons are present because of nonmonochromaticity of the pulse). The nature of these lower peaks is similar to that of the intrapeak structure in ATI spectra observed in [23], as was first shown in [24]. The one-photon peak at $E=E_1+\omega$ is not seen because its estimated height is about ten times smaller than the amplitude of oscillations in that energy region.

The third feature seen in Fig. 4, that requires some explanation, is oscillations of the envelope of the spectrum at higher energies. These oscillations come from the matrix element (54). Let $d_{\pm}(k)$ be the corresponding matrix element for the potential (50), i.e., be defined by Eq. (54) with integration extended from $-\infty$ to ∞. One could think that the difference between $d_{\pm}(k)$ and $d_{\pm}^{c}(k)$ becomes negligible for a sufficiently large cutoff radius X, but this is not always the case. Consider large values of k. Substituting in the first Born approximation $\varphi_{\pm}^{\text{out}}(x,k)\approx e^{\pm ikx}$ and retaining only the leading order term, one obtains

$$d_{\pm}(k)-d_{\pm}^{c}(k)\approx\ \mp 2iX\phi_0(X)\frac{\cos kX}{k}. \tag{56}$$

Because of the factor $\phi_0(X)$, this difference is indeed exponentially small in X, as expected, but it decays too slowly as a function of k. On the other hand, the dipole matrix element $d_{\pm}(k)$ decays faster than any exponential function, i.e., faster than e^{-ck} for any value of c, because stationary states in the potential (49) are entire functions of x. Hence at large k the cutoff dipole matrix element $d_{\pm}^{c}(k)$ is determined by the right-hand side of Eq. (56), which is an oscillating function of k. These oscillations are seen in the envelope of the spectrum in Fig. 4. They are clearly an artifact of the cutoff model (51). However, the calculations were done for this model, so they reproduce the oscillations, as they should. Note that the calculated results agree excellently with the predictions of perturbation theory over a huge dynamical range, which demonstrates high computational efficiency of the present approach.

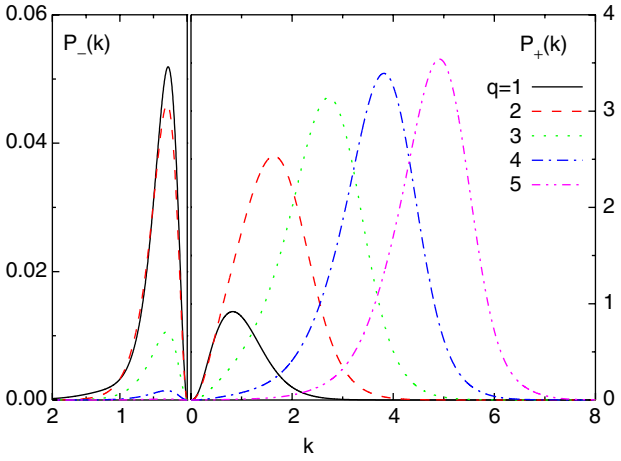

FIG. 5. (Color online) Spectra of particles ejected to the left, $P_-(k)$, and right, $P_+(k)$, in the sudden regime for several values of the momentum q transferred. Notice a big difference in scales in the left and right panels.

C. Sudden regime: The binary encounter peak

We now consider ionization by a large amplitude short pulse. In sudden approximation for the cutoff potential (51) one obtains [25]

$$P_{\pm}^{SA}(k) = \left| \int_{-X}^{X} \varphi_{\pm}^{\text{out}*}(x,k)(e^{iqx} - 1)\phi_0(x)dx \right|^2, \qquad (57)$$

where

$$q = F_0 \int_{-\infty}^{\infty} f(t)dt = F_0 T/2 \qquad (58)$$

is the momentum transferred to the particle by the pulse. In this case only the integral of the shape function $f(t)$ matters. In the calculations we define $f(t)$ by Eq. (52) with $\omega=0$, which leads to the second equality in Eq. (58).

First, we fixed $T=0.01$ and varied F_0 to obtain different values of q. Results of the calculations are shown in Fig. 5; they are indistinguishable to the scale of the figure from the results of sudden approximation (57). In the sudden regime, ionization to the left and right is highly asymmetric; this mimics the asymmetry of angular distribution in the three-dimensional case. The momentum transferred (58) is positive, so the pulse pushes the particle to the right, the direction in which ionization dominantly occurs. For example, for $q=1$, 3, and 5 total probabilities of ionization to the left are 4.0×10^{-3}, 8.8×10^{-4}, and 1.5×10^{-5}, and those to the right are 0.1720, 0.9424, and 0.9992, respectively. As q grows and becomes larger than the width of the momentum distribution in the initial state, about 1.5 in the present case, the position of the maximum of $P_+(k)$ approaches q and its shape approaches that of the momentum distribution. This is the binary encounter peak; a similar situation in the three-dimensional case was recently discussed in [26]. The spectrum of particles ejected to the left, $P_-(k)$, is determined by large momentum components in the initial state, so its height rapidly decays as q grows.

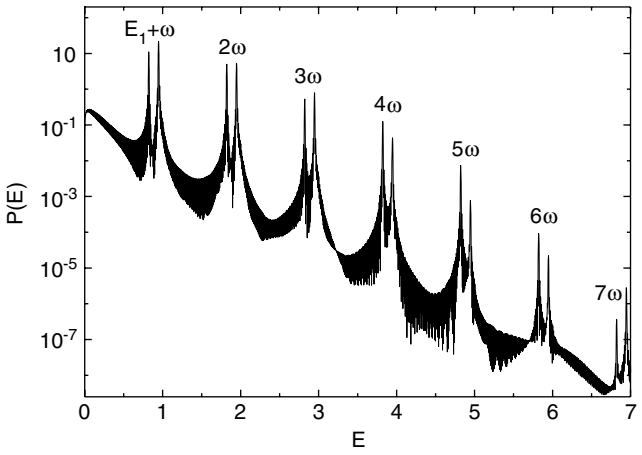

FIG. 6. The spectrum of ejected particles for a resonant field with $\omega=E_1-E_0=1$ and $F_0=0.2$. The ATI peaks at $E=E_1+n\omega$, $n=1,2,\ldots$, are clearly split into two Rabi components.

We have repeated the calculations, now keeping q fixed and increasing T. A visible departure from sudden approximation (57) occurs only for $T\approx1$. This is understandable, because the period of classical motion in the potential (49) with the ground state energy E_0 is 4.2. Further increase of T for a fixed q leads to the appearance of an interesting resonance structure corresponding to bouncing of the particle in the triangle well formed by the linear potential (51) at $|x|<X$ and zero potential at $|x|>X$, but this is an artifact of the cutoff model, so we shall not discuss it here.

D. Resonant field: Rabi doublets

Finally, we consider ionization by a resonant field, when rotating wave approximation [27] is expected to be valid. The excitation energy is $E_1-E_0=1$, so a resonance occurs in the interaction with a monochromatic field with frequency $\omega=1$. In the calculations, we use a finite length pulse,

$$f(t) = \begin{cases} \sin \omega t, & 0 \leqslant t \leqslant T, \\ 0, & \text{otherwise}, \end{cases} \qquad (59)$$

with $\omega=1$ and $T=100\times2\pi/\omega$, i.e., containing one hundred optical cycles. The calculations were done with $F_0=0.1$, 0.2, and 0.3; the results for $F_0=0.2$ are shown in Fig. 6. Even though spectra $P_-(k)$ and $P_+(k)$ in this case do not coincide, indicating strong departure from the perturbative regime, they are very close to each other near ATI peaks, so we again consider the distribution of ejected particles in energy (47). As is clear from the figure, the peaks are split into two components. Let us discuss the origin of this splitting.

The relevant model is a two-level atom in a resonant field [27] with zero detuning, $\omega=E_1-E_0$. For direct ionization from the ground state the particle must absorb at least two photons. Assuming that this process is much less probable than one-photon ionization from the excited state, to account for ionization in the two-level model the upper state should be assigned a width Γ. Then the probability to survive in bound states decays as $e^{-\Gamma t/2}$. Total ionization probabilities P_{ion} obtained with $F_0=0.1$, 0.2, and 0.3 are 0.10, 0.54, and

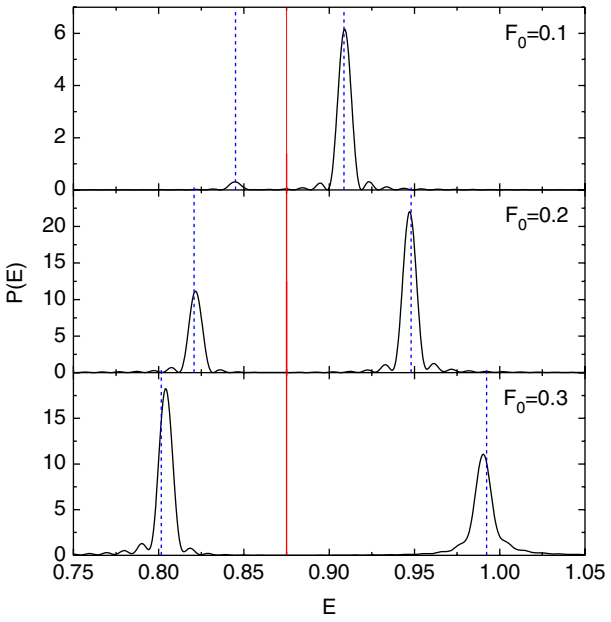

FIG. 7. (Color online) Detailed structure of the first Rabi doublet for three values of F_0. The vertical solid line indicates position of the one-photon absorption energy $E_1+\omega$. Vertical dashed lines show energies calculated from Eq. (62) with $n=1$; an additional small constant 6×10^{-4} was added to Eq. (62) to account for a shift caused by a finite spectral width of the pulse.

0.94, which via $P_{\text{ion}}=1-e^{-\Gamma T/2}$ corresponds to $\Gamma=3.3\times10^{-4}$, 2.4×10^{-3}, and 8.6×10^{-3}, respectively. In the presence of the field, the upper weakly bound level acquires a dynamical Stark shift which could be safely estimated as $F_0^2/4\omega^2$ [21]. In addition, the field causes its splitting into two "dressed" components shifted by $\pm\Omega$, where Ω is the Rabi frequency,

$$\Omega=[|F_0 d_{10}/2|^2-(\Gamma/4)^2]^{1/2}, \tag{60}$$

and d_{10} is the dipole matrix element (its numerical value is not affected by the difference between (50) and (51) discussed in the end of Sec. V B),

$$d_{10}=\int \phi_1(x)x\phi_0(x)dx=0.636. \tag{61}$$

One can see that in all the cases the first term in Eq. (60) is by far dominant. Summarizing, ionization occurs from the upper level populated via its mixing with the ground state by the resonant field, which should result in the appearance of multiphoton Rabi doublet peaks in the ionization spectrum at energies

$$E_{n\pm}=E_1+n\omega+F_0^2/4\omega^2\pm\Omega, \quad n=1,2,\ldots . \tag{62}$$

This interpretation is confirmed in Fig. 7. Here, we show the first doublet, $n=1$, for three values of F_0. Equation (62) reproduces very well positions of the peaks: not only linear in F_0 Rabi splitting Ω, but also the quadratic dynamical Stark shift must be taken into account to obtain such an agreement with the calculated results. Note that splitting seems to grow slower with F_0 than Ω, which might be a quadratic effect. The ratio of the heights of peaks within a doublet, see Fig. 7, as well as between doublets, strongly depends on F_0. In particular, for $F_0=0.3$ the first doublet is lower than the second one.

A related effect caused by off-resonance (large detuning) strong coupling between the ground and first excited states in cesium was experimentally observed in [28]. There are also a number of theoretical papers where similar doublet substructures in ATI peaks were predicted and analyzed [29–31]. In the present simple model the effect of Rabi splitting of ATI peaks is clearly demonstrated and its interpretation given above leaves no ambiguities.

VI. CONCLUSIONS AND PERSPECTIVES

The key property of the approach originally proposed in [2] for the radial problem and extended here to the whole-axis problem is that it treats continuum on equal footing with discrete spectrum. An advantage of this approach over the direct numerical solution of TDSE stems from the fact that the outgoing wave boundary conditions are exactly incorporated in the formulation. Hence in the calculations it is sufficient to consider only a small region of configuration space where the interaction takes place, and there are no limitations on the duration of the interaction in time because no artificial reflection from the boundaries occurs. The numerical efficiency of this approach was demonstrated by calculations presented in [2] and above; a more realistic physical model will be considered in the forthcoming paper [17].

The main obstacle in the application of the present approach to practical problems is that so far the stationary theory of Siegert pseudostates has been developed only for s-wave scattering in one-channel [4] and two-channel [5] cases. The extension of the present approach to the three-dimensional case is a priority task. To this end, the formulation of [4] must be generalized to nonzero angular momenta. This is doable, the work is in progress. A generalization to a multichannel case is also of interest, however, before that a nonstationary theory for the two-channel case [5] is to be developed, which seems to be more or less straightforward.

Finally, the present approach opens the way for the analytical treatment of transitions to continuum in nonstationary quantum systems in adiabatic approximation. This interesting development will be a subject of the third paper of this series.

ACKNOWLEDGMENTS

I thank T. Morishita for useful discussions of the physics of laser-atom interaction.

[1] A. J. F. Siegert, Phys. Rev. **56**, 750 (1939).
[2] O. I. Tolstikhin, Phys. Rev. A **73**, 062705 (2006).
[3] O. I. Tolstikhin, V. N. Ostrovsky, and H. Nakamura, Phys. Rev. Lett. **79**, 2026 (1997).
[4] O. I. Tolstikhin, V. N. Ostrovsky, and H. Nakamura, Phys. Rev. A **58**, 2077 (1998).
[5] G. V. Sitnikov and O. I. Tolstikhin, Phys. Rev. A **67**, 032714 (2003).
[6] O. I. Tolstikhin, I. Yu. Tolstikhina, and C. Namba, Phys. Rev. A **60**, 4673 (1999).
[7] O. I. Tolstikhin, V. N. Ostrovsky, and H. Nakamura, Phys. Rev. A **63**, 042707 (2001).
[8] E. L. Hamilton and C. H. Greene, Phys. Rev. Lett. **89**, 263003 (2002).
[9] K. Toyota and S. Watanabe, Phys. Rev. A **68**, 062504 (2003).
[10] V. Kokoouline and C. H. Greene, Phys. Rev. Lett. **90**, 133201 (2003); Phys. Rev. A **68**, 012703 (2003); **69**, 032711 (2004).
[11] G. V. Sitnikov and O. I. Tolstikhin, Phys. Rev. A **71**, 022708 (2005).
[12] V. N. Ostrovsky and N. Elander, Phys. Rev. A **71**, 052707 (2005); Chem. Phys. Lett. **411**, 155 (2005).
[13] K. Toyota, T. Morishita, and S. Watanabe, Phys. Rev. A **72**, 062718 (2005).
[14] S. Yoshida, S. Watanabe, C. O. Reinhold, and J. Burgdörfer, Phys. Rev. A **60**, 1113 (1999).
[15] S. Tanabe, S. Watanabe, N. Sato, M. Matsuzawa, S. Yoshida, C. Reinhold, and J. Burgdörfer, Phys. Rev. A **63**, 052721 (2001).
[16] R. Santra, J. M. Shainline, and C. H. Greene, Phys. Rev. A **71**, 032703 (2005).
[17] K. Toyota *et al.* (unpublished).
[18] C. Bloch, Nucl. Phys. **4**, 503 (1957).
[19] R. G. Newton, *Scattering Theory of Waves and Particles* (Springer-Verlag, New York, 1982).
[20] L. D. Landau and E. M. Lifshitz, *Quantum Mechanics (Non-relativistic Theory)* (Pergamon Press, Oxford, 1977).
[21] N. B. Delone and V. P. Krainov, *Atoms in Strong Light Fields*, Springer Series in Chemical Physics (Springer, New York, 1985).
[22] P. Agostini, F. Fabre, G. Mainfray, G. Petite, and N. K. Rahman, Phys. Rev. Lett. **42**, 1127 (1979).
[23] R. R. Freeman, P. H. Bucksbaum, H. Milchberg, S. Darack, D. Schumacher, and M. E. Geusic, Phys. Rev. Lett. **59**, 1092 (1987).
[24] J. H. Eberly and J. Javanainen, Phys. Rev. Lett. **60**, 1346 (1988).
[25] A. M. Dykhne and G. L. Yudin, Usp. Fiz. Nauk **125**, 377 (1978) [Sov. Phys. Usp. **21**, 549 (1978)].
[26] D. Dimitrovski, E. A. Solov'ev, and J. S. Briggs, Phys. Rev. A **72**, 043411 (2005).
[27] L. Allen and J. H. Eberly, *Optical Resonance and Two-Level Atoms* (Dover, New York, 1987).
[28] W. Nicklich, H. Kumpfmüller, H. Walther, X. Tang, H. Xu, and P. Lambropoulos, Phys. Rev. Lett. **69**, 3455 (1992).
[29] X. Tang, A. Lyras, and P. Lambropoulos, J. Opt. Soc. Am. B **7**, 4 (1990).
[30] C. Meier and V. Engel, Phys. Rev. Lett. **73**, 3207 (1994).
[31] A. Adler, A. Rachman, and E. Robinson, J. Phys. B **28**, 5057 (1995), **28**, 5077 (1995).